ACS SENSORS

Article

Cite This: ACS Sens. 2019, 4, 1899−1908

pubs.acs.org/acssensors

Near-Infrared Broadband Cavity-Enhanced Spectroscopic Multigas Sensor Using a 1650 nm Light Emitting Diode

Kaiyuan Zheng,[†] Chuantao Zheng,*[,†] Ningning Ma,[†] Zidi Liu,[†] Yue Yang,[†] Yu Zhang,[†] Yiding Wang,[†] and Frank K. Tittel[‡]

[†]State Key Laboratory of Integrated Optoelectronics, College of Electronic Science and Engineering, Jilin University, 2699 Qianjin Street, Changchun, 130012, P.R. China

[‡]Department of Electrical and Computer Engineering, Rice University, 6100 Main Street, Houston, Texas 77005, United States

Supporting Information

ABSTRACT: A near-infrared broadband cavity-enhanced sensor system was demonstrated for the first time using an energy-efficient light emitting diode (LED) with a central emission wavelength at 1650 nm and a light power of ∼16 mW. A portable absorption gas cell was designed for realizing a compact and stable optical system for easy alignment. An ultrashort 8-cm-long cavity was fabricated consisting of two mirrors with a ∼99.35% reflectivity. Methane (CH_4) measurement was performed employing two detection schemes, i.e., NIRQuest InGaAs spectrometer and scanning monochromator combined with phase-sensitive detection. Retrieval of CH_4 concentration was performed using a least-squares fitting algorithm. Sensitivities (i.e., minimum detectable absorption coefficient) were achieved of 1.25×10^{-6} cm^{-1} for an averaging time of 45 s using the NIRQuest InGaAs spectrometer and 1.85×10^{-6} cm^{-1} for an averaging time of 8 min using the scanning spectrometer in combination with lock-in detection. Field monitoring of CH_4 gas leakage was performed using the NIRQuest spectrometer. Multigas sensing of CH_4 and acetylene (C_2H_2) was carried out simultaneously using the high-resolution scanning spectrometer. A linear response of the retrieved concentration level versus nominal value was observed with a large dynamic range, demonstrating the reliability of the compact LED-based near-infrared broadband cavity-enhanced absorption spectroscopy (NIR-IBBCEAS) for multigas sensing applications.

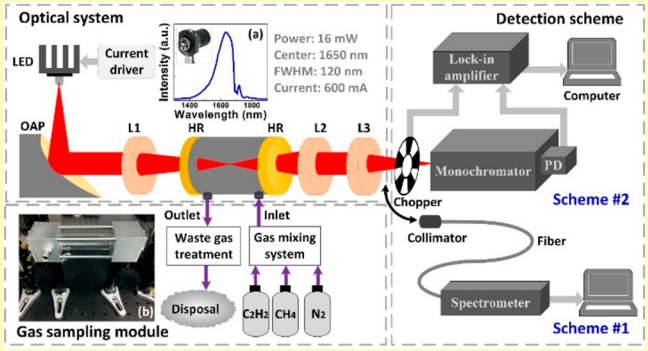

KEYWORDS: *gas sensor, infrared absorption spectroscopy, incoherent broadband cavity-enhanced absorption spectroscopy, acetylene detection, methane detection, light emitting diode*

Chemical gas-phase analysis is significant in physics, chemistry, space science, industrial process control, as well as in atmospheric applications.[1−4] Fundamental requirements for chemical analysis and gas sensing include sensitivity, selectivity, portability, and affordability.[5−8] Incoherent broadband cavity-enhanced absorption spectroscopy (IBBCEAS)[9−11] meets these criteria, as it is simple, robust, and ideal for portable application. Furthermore, IBBCEAS offers high sensitivity and allows for selective multicomponent measurement due to the broad bandwidth of the light source. For example, *in situ* measurements of multiple gases in the visible spectral range were reported using this technique.[12,13]

Recent developments of broadband light sources operating in the near-infrared (NIR) allow extension of precise spectroscopic measurements of the molecular vibrational overtones region using IBBCEAS. In 2008, Orphal et al. developed an NIR-IBBCEAS setup in combination with a Fourier-transform spectrometer to explore the high-resolution molecular spectroscopy of carbon dioxide (CO_2), carbonyl sulfide (OCS), and semiheavy water ($HD^{18}O$) in the NIR region.[14] In 2009, Denzer et al. demonstrated a fiber coupled NIR superluminescent light emitting diode (SLED) using a 25-cm-long cavity with mirrors of reflectivity 99.98%, and sensitivities were achieved of 6.1×10^{-8} cm^{-1} using the dispersive spectrometer in combination with phase-sensitive detection, and 1.5×10^{-8} cm^{-1} using the Fourier transform interferometer.[15] In 2011, the same group proposed an NIR-IBBCEAS system using a supercontinuum (SC) source, and a sensitivity of 4×10^{-9} cm^{-1} was obtained for a 4 min averaging time.[16] In 2015, Chandran et al. reported a SC-based NIR-IBBCEAS setup to record the absorption of 1,4-dioxane using a 644-cm-long cavity consisting of two highly reflective mirrors (99.9%), leading to a detection limit of 8×10^{-8} cm^{-1} in a 120 min averaging time.[17] In 2018, Prakash et al. developed a NIR-IBBCEAS sensor for the detection of natural gas mixtures, and

Received: April 29, 2019
Accepted: June 11, 2019
Published: June 11, 2019

DOI: 10.1021/acssensors.9b00788
ACS Sens. 2019, 4, 1899−1908

a detection limit (3σ) of 460 ppmv, 141 ppmv, 175 ppmv, and 173 ppmv for methane (CH_4), butane (C_4H_{10}), ethane (C_2H_6), and propane (C_3H_8), respectively, was achieved.[18] In our previous work, an NIR-IBBCEAS sensor system in combination with a Fourier-transform spectrometer was developed for high-resolution CH_4 detection. A 40-cm-long cavity formed by two highly reflective mirrors (99.94%) was used and a detection sensitivity of 4.6×10^{-7} cm^{-1} was achieved.[19]

The light sources commonly used in NIR-IBBCEAS include SC sources[17,20,21] and xenon lamps,[18,19] and they are generally costly, require high-power consumption, and are too cumbersome to use in a portable device. Additionally, these types of broadband light sources generate an ultrawide emission spectrum, generally ranging from the visible to the mid-infrared (usually covering 1500−2000 nm), far beyond the spectral coverage of the highly reflective (HR) dielectric mirrors (usually covering 200−400 nm). Therefore, optical filters with different cutoff frequencies are needed to match the light emitting spectrum with the highly reflective region of the cavity, leading to the attenuation of light intensity due to the imperfect transmittance of the filters. Furthermore, because the emission spectrum of the SC source (up to several hundred nanometers) is much wider than the LED source (tens of nanometers), the spectral density of the former source will be much weaker than the latter one under the same power level. This could result in a waste of spectrum and power for the SC source used in IBBCEAS.

In recent years, as potential light source alternatives in NIR-IBBCEAS, some kinds of infrared LEDs were reported, such as the PbSe-based Quantum dot-LED (QD-LED),[22,23] polymer-LED (PLEDs),[24] superluminescent-LED (SLED),[15,20] and InGaAs-LED.[25,26] These LED sources offer different advantages and disadvantages in terms of light power, robustness, portability, and cost. PbSe-based QD-LEDs have easily tunable emission wavelength as well as high quantum yield. However, the low external quantum efficiency (EQE) of these LEDs restricts their application because of the nonradiative recombination caused by the aggregation in the solid-state QD films.[23] PLEDs can tune over the entire visible region to the NIR range by incorporating different narrow band gap monomers into the polyfluorene backbone. Nevertheless, the stability and luminescent quenching at high current density are still questionable.[24] SLED is a high-power (~40 mW), broadband superluminescent diode with a near Gaussian spectral profile and low ripple, but lacks cost-efficiency. InGaAs-based LED is stable, inexpensive, and possesses relatively high output power (~10 mW) but lacks good beam quality, narrow line width, and tunability compared with laser sources.[25] Therefore, due to the above limitations, especially the low optical power, infrared LEDs were rarely used in the NIR-IBBCEAS.

In order to overcome these limitations and take advantage of a low-cost, power-efficient, compact, and long-lived InGaAs-based LED, for the first time to the best of our knowledge, we demonstrate an LED-based NIR-IBBCEAS for multigas sensing. The broadband LED emitting at a central wavelength of ~1650 nm and a full width at half-maximum (fwhm) of 120 nm within the highly reflective range (1500−1800 nm), significantly reduces the waste of LED power and emission spectra. A portable cage-based absorption gas cell with a cavity length of 8 cm and a volume of 42 mL was developed. Two measurement schemes, i.e., NIRQuest InGaAs spectrometer and scanning monochromator were comparably employed for CH_4 detection. Simultaneous detection of CH_4 and acetylene (C_2H_2) in the laboratory was conducted to prove the ability of the sensor system for multigas sensing. A field deployment of the sensor system for monitoring CH_4 leakage was carried out to verify the usability of the sensor. The proposed sensor system provides an effective tool for sensitive and multiple gas species sensing with a compact and inexpensive package.

SENSOR SYSTEM STRUCTURE AND DESIGN

Sensor System Structure. The sensor structure is illustrated in Figure 1. A NIR LED (M1650L4, Thorlabs, USA) emitting at a central wavelength of ~1650 nm with a 120 nm fwhm was used as the broadband light source. The NIR LED was mounted on an aluminum heat sink to stabilize its output optical intensity and spectral distribution. The LED emission spectra with its photograph are shown in Figure 1a. The LED emission light was collimated by an off-axis parabolic (OAP) mirror. Since the focus configuration is much more effective than the parallel arrangement in the cavity coupling method,[10] the collimated light beam was therefore focused into the center of an optical cavity using a plano-convex lens coated over the 1.1−1.8 μm range. The beam propagated through an ultrashort 8-cm-long optical cavity consisting of two reflective mirrors (99.3−99.4% @ 1500−1800 nm, Layertec GmbH, Germany) with a radius of curvature (RoC) of 20 cm. In order to achieve good sensitivity, highly reflective mirrors are preferred in NIR-IBBCEAS. However, through experiment, an ultrahigh reflectivity resulted in a low coupling efficiency between the used NIR LED and the cavity due to the incoherence characteristics and large beam divergence of the LED. This is not a problem for fiber coupled NIR SLED devices where the radiation emerges from the fiber spatially coherent. Therefore, cavity mirrors with modest reflectivity are suitable for the NIR LED based IBBCEAS. That is why two mirrors with a reflectivity of 99.35% were used in this work. It is unnecessary to spatially match the LED beam to the fundamental TEM_{00} mode of the cavity. Broadband incoherent light contains the frequency components that correspond to the eigen-modes of a cavity for a given geometry. So, a certain fraction of the LED light will couple into the cavity and the

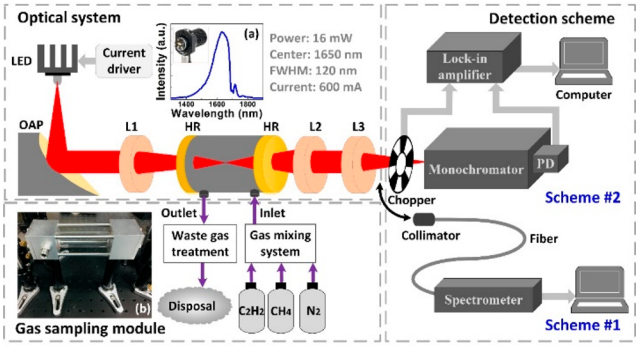

Figure 1. Structure of the LED-based NIR-IBBCEAS sensor system, including an optical system, a gas sampling module, and two detection schemes. (a) LED emission spectrum versus wavelength in the NIR range with an inset photograph of the LED. (b) Photograph of the fabricated cavity with dimensions of $4.5 \times 12 \times 4.5$ cm^3. OAP: off-axis parabolic mirror for collimation. L1, L2, and L3: achromatic lenses with different focal lengths. HR: highly reflective mirror. PD: photodetector. Inlet and outlet: gas channels of the absorption cell.

DOI: 10.1021/acssensors.9b00788
ACS Sens. 2019, 4, 1899−1908

injected LED light will excite all accessible axial and transverse modes of the cavity for a given excitation conditions. This is desirable and advantageous for broadband cavity-enhanced operation, leading to a dense quasi-continuous transmission at the whole wavelength region.[21] A photograph of the designed cavity is shown in Figure 1b, which has an inlet and outlet at either end. Gas samples were diluted from a standard 2000 parts-per-million in volume (ppmv) C_2H_2 sample and a 10 000 ppmv CH_4 sample in nitrogen (N_2) using a standard gas mixing system (Series 4000, Environics, USA). The cavity output was then collimated and focused onto two detection devices with different measurement schemes. One was focused into a fiber collimator and then coupled to a computer-controlled near-IR spectrometer (NIRQuest256−2.1, Ocean optics, USA) via a multimode optical fiber (600 μm in diameter). The light intensity was detected by an InGaAs array photodetector, and the spectrometer which consists of an entrance slit, grating, and array has a spectral resolution of 7.6 nm. The other was focused onto the entrance slit of a scanning monochromator (Omni-λ300, Zolix) with 1200 grooves/mm grating, and the light intensity was detected with a near-IR InGaAs photodetector. Lock-in detection was used to improve the signal-to-noise ratio (SNR), using a lock-in amplifier (SR830, Stanford Research Systems) with a mechanical chopper (SR540, Stanford Research Systems).

As demonstrated in Figure 2, the divergence angle of the NIR LED was 20°, and an OAP mirror with a focal length of

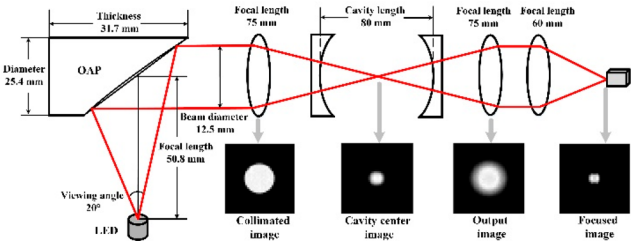

Figure 2. Light transmission diagram of the optical system. Insets are the simulated images of collimated cavity input beam, cavity central beam, cavity output beam, and focused beam for detection, respectively.

50.8 mm and a diameter of 25.4 mm was used to collimate the light beam, and thus a round-shape beam with a diameter of 12.5 mm was obtained, which is smaller than the diameter of the reflective mirrors (12.7 mm). After carefully adjusting the position of the two reflective mirrors, the light beam was focused into the center of the cavity by a plano-convex lens with a focal length of 75 mm. The cavity output was collimated (75 mm in focal length) and focused (60 mm in focal length) by two achromatic lenses. Compared to an aspheric lens, an achromatic lens can achieve a tighter focus and a better off-axis performance, and can keep a nearly constant focal length across a wide wavelength range. Simulated images of the collimated beam before coupling into the cavity, the beam at the cavity center, the cavity output beam, and the beam focused to the spectrometer are shown in the inset of Figure 2, which indicates the focus operation of the cavity coupling structure. The focused image is a square shape, which is a projection of the LED chip with a size of 1 mm × 1 mm.

Absorption Gas Cell Design. The computer aided design (CAD) image of the portable absorption gas cell is shown in Figure 3a. The absorption cell possesses a dimension size of

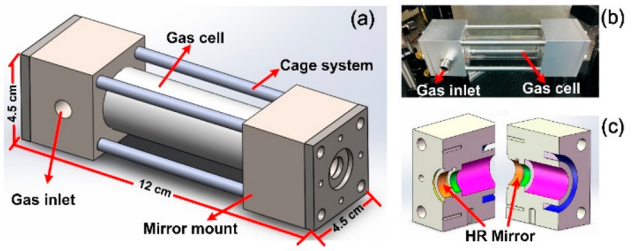

Figure 3. (a) CAD image of the compact absorption gas cell with dimensions of length (12 cm), width (4.5 cm), and height (4.5 cm). (b) Photograph of the fabricated absorption gas cell. (c) CAD image of the mirror mounts used to install and seal the highly reflective mirrors (HR Mirror).

4.5 × 12 × 4.5 cm^3 and a mass of 0.5 kg, which consists of a gas cell, a cage system, and two custom-made mirror mounts. The cavity length is 8 cm and the cell volume is 42 mL. A gas inlet and outlet (not shown in Figure 3a) are located in the front and in the rear of the cell, respectively. The cage system with good stability and robustness is designed for a simple alignment and rapid adjustment of the cavity length without affecting the collimation performances. Figure 3c shows the self-designed mirror mount used to install the highly reflective mirrors. Two sealing rings are placed at both ends of the mirror. A 1-cm-long hole was designed between the gas cell and the mirror mount to adjust the cavity length and the incidence angle of the beam for achieving the optimal SNR. Figure 3b shows the photograph of the fabricated and sealed absorption gas cell. The fabricated absorption cell was made of aluminum and glass, which was used for gas detection under atmospheric pressure in this work. The fabricated compact gas cell with a small volume is particularly suitable for size- and weight-limited applications, such as balloon-embedded observation, and also it is ideal for mobile measurements of atmospheric gas detection.

Mirror Reflectivity Calibration. The sensor system was first calibrated by measuring the wavelength-dependent mirror reflectivity to determine the absorption coefficient of the target gas species.[22] We used the standard CH_4 (5000 ppmv) and C_2H_2 (1000 ppmv) samples balanced with N_2 to calibrate the mirror reflectivity,[18] which could be calculated by eq 1

$$R(\lambda) = 1 - \sigma(\lambda)nd\left(\frac{I}{I_0 - I}\right) \quad (1)$$

where I and I_0 are the measured light intensity for a definite cavity length d (cm) when the cavity is filled with target gas and pure N_2, respectively. n (molecules per cm^3) represents the number density; $\sigma(\lambda)$ (cm^2 per molecules) is the reference absorption cross section of the target gas, which is available from the high-resolution transmission (HITRAN) absorption database. The corresponding cross sections were convolved to the instrument resolution (NIRQuest spectrometer, 7.6 nm). Then, $R(\lambda)$ was calculated as a function of wavelength, which was further interpolated and fitted using a second-order polynomial.[18] The wavelength-dependent reflectivity of the cavity mirror was therefore acquired. More details of the mirror calibration section were shown in the Supporting Information. As depicted in Figure S4, the maximum value of $R(\lambda)$ is calibrated to be 99.35%, and thus an effective path length $L_{eff} = d/(1 - R)$ of 12.3 m was obtained with a cavity length of 8 cm.

DOI: 10.1021/acssensors.9b00788
ACS Sens. 2019, 4, 1899−1908

For a high-power wideband light source, much more light will transmit through the cavity on either side of the mirror stop band, and this leads to the saturation of the NIRQuest spectrometer with an InGaAs-array detector, which is essentially a "stray light" problem. The NIRQuest spectrometer is a simple design and cannot cope when the useful light levels of a few hundred nanowatts are swamped by light that passes the edge of the mirror stop band, and perhaps a few hundred microwatts light level is scattered inside the spectrometer due to the imperfect optics configuration. Furthermore, the sensor can make full use of the luminous spectrum of the LED whose emitting spectra is within the highly reflective range of the cavity mirror, as shown in Figure 4. This results in a high utilization of the light source without any waste of the LED spectra.

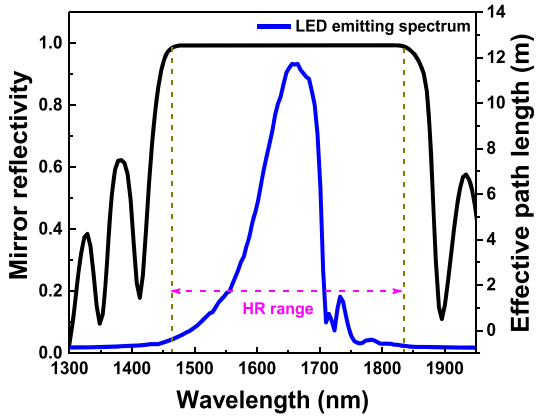

Figure 4. Modeled mirror reflectivity with its effective path length (black line). The calibrated mirror reflectivity from the experimental measurement in the 1500−1700 nm retrieval range is shown in the Supporting Information.

Concentration Retrieval Method. The spectral output of the cavity was first calibrated with only N_2 passing through the cavity with no absorption, and a second measurement was subsequently performed using the target gas with a definite concentration level. The absorption coefficient α for the target gas is expressed as[13]

$$\alpha = \sigma \cdot n \tag{2}$$

The concentration retrieval of the target gas is performed using a least-squares fitting algorithm, expressed as

$$\alpha = \sum_i n_i \sigma_i(\lambda)(s + t\lambda) + p\lambda^2 + q\lambda + r \tag{3}$$

where n_i represents the fitting coefficients of different gas species, s and t are the shift and squeeze values of the reference absorption spectra to correct the wavelength calibration, respectively; $p\lambda^2 + q\lambda + r$ accounts for the background effects resulting from the LED emission fluctuation, mechanical vibration, and system drift.

The uncertainties in the reference cross sections were analyzed using the standard approach for the propagation of error.[27] The uncertainties arise from the pressure error (1.3%), the temperature error (1%), the wavelength calibration (1.2%), and the convolution between the high-resolution spectrum and instrumental function (1%). Hence, the uncertainty associated with the reference cross section was found to be ∼2.2%.[18] Several ways can be used to get the accurate reference cross section. By stabilizing the pressure and temperature of the gas cell and using these parameters in the HITRAN simulation, the high-resolution absorption cross section under this environmental condition can be obtained. In addition, calibration of the spectrometer is necessary in order to obtain an accurate mapping relationship between the wavelength and light intensity, and thereby a more accurate convolution result can be acquired. Furthermore, eliminating the possible interferences with other molecular absorptions, such as CO_2 and H_2O, can also be helpful to obtain an accurate reference cross section.

SINGLE-GAS SENSING PERFORMANCE OF CH_4

CH_4 Measurement Using NIRQuest Spectrometer. The NIRQuest spectrometer was configured with a 100 lines/mm grating, a thermo-electric cooled (TEC) InGaAs-array detector (Hamamatsu G9206−256W), and a 25 μm slit, which yielded a spectral range of 900−2050 nm and an optical resolution of 7.6 nm. In this detection scheme, the integration time was set to 100 ms and the averaging number was set to 10, thus a sampling interval of 1 s was required to obtain an absorption spectrum.

Retrieval of the CH_4 concentration level was performed by fitting the experimentally measured absorption coefficient α with eq 2 and eq 3 using a least-squares algorithm. In the fitting procedure, CH_4 absorption line strength in the spectral range of 1610−1690 nm can be available from the HITRAN 2012 database and the Voigt broadening of the CH_4 absorption line at 300 K and 760 Torr was taken into consideration. Figure 5 shows the comparison between the measured and fitted absorption coefficient of CH_4 for a nominal concentration level of 5000 ppmv in balance with N_2, and a good agreement between the measured and fitted data is observed. The SNR of the CH_4 absorption spectrum can be estimated from the ratio between the maximum absorption difference and the standard deviation of the residual. Therefore, a SNR of 40 was deduced from the raw absorption spectra, indicating a detection precision of 125 ppmv in a 1 s sampling time for CH_4 measurement.

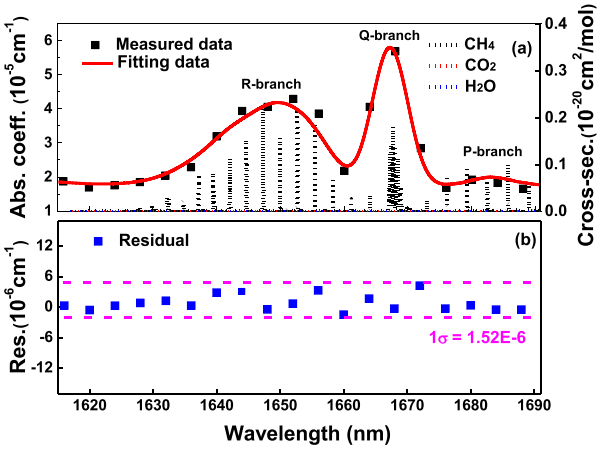

Figure 5. (a) Comparison between the measured (black dot) and the modeled (red line) absorption spectra of 5000 ppmv CH_4 from 1610 to 1690 nm. Short dots represent the high-resolution absorptions of CH_4, CO_2, and H_2O. (b) Residual between the measured absorbance and the fitted value with a standard deviation of 1.52×10^{-6} cm^{-1}.

DOI: 10.1021/acssensors.9b00788
ACS Sens. 2019, 4, 1899−1908

Then, we calibrated the sensor by measuring the CH_4 samples with different concentration levels, as depicted in Figure 6. Concentration retrieval was carried out in the range of 1610−1690 nm. The inset of Figure 6 shows the retrieved concentration results as a function of the nominal gas concentration levels generated by the Environics gas mixing system. A linear response (R^2 = 0.997) is found for CH_4 detection, which validates the accuracy of the LED-based NIR-IBBCEAS and proves the feasibility of this method for gas sensing applications.

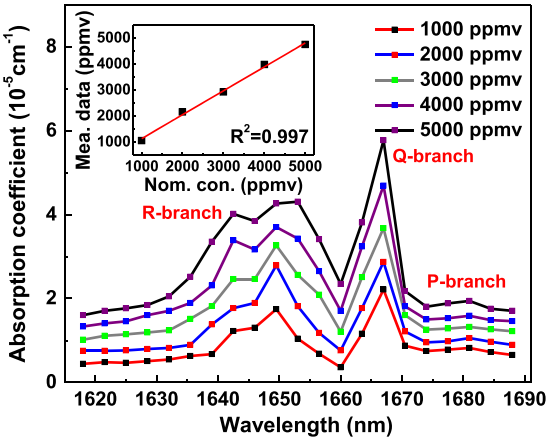

Figure 6. Measured absorption coefficient of the CH_4 samples with different mixing ratios from 1000 to 5000 ppmv in the spectral range of 1610−1690 nm. The inset shows the results of the measured CH_4 concentration versus the nominal concentration generated by the Environics gas mixing system.

The effects of H_2O on CH_4 concentration retrieval in the spectral range of 1600−1700 nm were analyzed. We assume a relative humidity of 95% at 300 K corresponding to a H_2O concentration of 3%. When we used the NIRQuest spectrometer to retrieve the CH_4 concentration with a low level of 120 ppmv (i.e., the limit of detection), the retrieved CH_4 concentration was 119.8 ppmv (relative error ∼0.16%). Using the scanning spectrometer to retrieve the CH_4 concentration with a low level of 28.4 ppmv (i.e., the limit of detection), the retrieved CH_4 concentration was 28.36 ppmv (relative error ∼0.14%). Thus, the interference of H_2O is negligible. The effects of atmospheric CO_2 on CH_4 concentration retrieval in the spectral range of 1600−1700 nm were then analyzed. We assume a normal CO_2 concentration level of 330 ppmv at 300 K. Using the NIRQuest spectrometer to retrieve the CH_4 concentration with a low level of 120 ppmv (i.e., the limit of detection), the retrieved CH_4 concentration was 119.7 ppmv (relative error ∼0.25%). When we used the scanning spectrometer to retrieve the CH_4 concentration with a low level of 28.4 ppmv (i.e., the limit of detection), the retrieved CH_4 concentration was 28.35 ppmv (relative error ∼0.17%). Thus, the interference of CO_2 is negligible. The absorption of the atmospheric CO_2 and H_2O levels is relatively small compared to CH_4 (∼120 ppm level) in the spectral range of 1600−1700 nm. In addition, since the CH_4 concentration retrieval is performed over a wide spectral range, the impact of CO_2 and H_2O on the broadband retrieval of CH_4 concentration can be neglected.

An Allan-Werle variance analysis was performed to evaluate the long-term stability and precision of the CH_4 sensor system. By passing pure N_2 into the gas cell at a flow rate of 300 sccm, the concentration levels of CH_4 were recorded for 250 consecutive spectra with a sampling interval of 1 s within the 1610−1690 nm range. As depicted in Figure 7, the Allan deviation is plotted on a log−log scale versus the averaging time, a limit of detection (LoD) of 120 ppmv is obtained for an averaging time of 1 s. When the averaging time increases to 45 s, the LoD is decreased to 19.4 ppmv. A continuous decrease similar to the decrease of the curve of ∼sqrt ($1/\tau$) is observed as the averaging time increases, indicating a white noise dominated sensor system when the averaging time is <45 s.

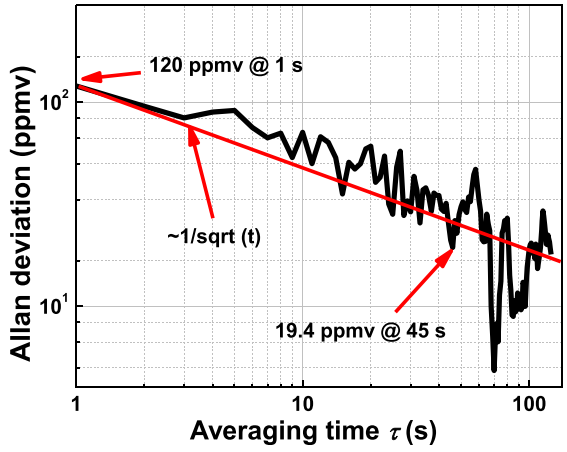

Figure 7. Allan deviation plot as a function of averaging time. The Allan variance analysis shows a minimum value for an averaging time of 45 s, indicating the optimal sensitivity.

CH_4 Measurement Using Scanning Spectrometer and Lock-In Detection. A scanning spectrometer in conjunction with lock-in detection was used to optimize the measurement of broadband absorption features. Since only a small fraction of the LED power transmitted through the highly reflective cavity, a lock-in amplifier with an integration time of 1 s and a mechanical chopper operated at 245 Hz were used to improve the SNR. The dispersion of this monochromator was 2.7 nm/mm with a 1200 lines/mm grating, and the exit slit width was adjusted to 150 μm yielding a resolution of 0.4 nm. The wavelength scanning was performed with a step of 0.1 nm, and therefore a complete measurement time of ∼8 min was acquired to obtain an absorption spectrum.

In order to evaluate the sensor performance using the lock-in assisted scanning spectrometer, the absorption spectrum of CH_4 with 4600 ppmv concentration level in the weak $2\nu_3$ overtone transitions range was measured. Figure 8 shows the measured absorption coefficient at a standard atmospheric pressure together with the modeled least-squares fitting curve, where the modeled spectrum agrees well with the measured data. Furthermore, a SNR of 162 ($3.1 \times 10^{-4}/1.91 \times 10^{-6}$) and a detection precision of 28.4 ppmv (4600/162) were obtained using this detection scheme. The detection limit can be generalized by calculating the minimum detectable absorption coefficients for equivalent single-wavelength measurements using the strongest line in the fitting range.[20] In the $2\nu_3$ band, the obtained strongest line has an absorption cross section of 2.61×10^{-21} cm^2/molecules on the Q-branch of CH_4 under the condition of the spectral resolution of 0.4 nm. Thus, a detection sensitivity of 1.85×10^{-6} cm^{-1} was achieved with a measurement time of 8 min. Moreover, the limit of detection can also be estimated by $3.1 \times 10^{-4}/162 = 1.91 \times$

DOI: 10.1021/acssensors.9b00788
ACS Sens. 2019, 4, 1899−1908

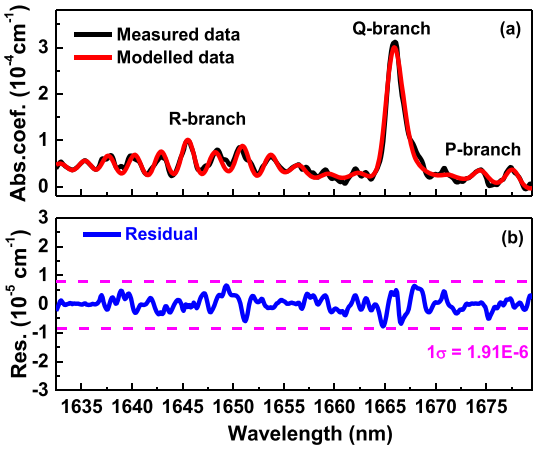

Figure 8. (a) Experimental high-resolution absorption spectrum measured with the lock-in detection assisted scanning spectrometer from a 4600 ppmv CH_4 sample (black line) together with the modeled least-squares fitting curve (red line). (b) Residue and the standard deviation of the residual spectrum is 1.91 × 10^{-6} cm^{-1}.

10^{-6} cm^{-1}. The two values (1.85 × 10^{-6} and 1.91 × 10^{-6} cm^{-1}) show good consistency, and the slight difference between these two values was probably caused by the fitting error of the absorption profile.

Different CH_4 concentration levels balanced with pure N_2 (1000, 2000, 3000, 4000 ppmv) were used to calibrate the sensor, as depicted in Figure 9a. Four strong absorption peaks (1642.8 nm, 1645.5 nm, 1648.2 nm, and 1650.8 nm, noted as peak1, peak2, peak3, and peak4) in the fitting range of 1642–1651 nm were selected for concentration determination. The inset of Figure 9a shows a good linear relationship (R^2 = 0.994) between the measured and nominal concentration levels. Furthermore, Figure 9b,c,d,e describes the relationship between the maximum absorption coefficient (α_{max}) at the four peaks and the measured concentration. Linear dependence was found between α_{max} and the CH_4 concentration level in the four curves, indicating the feasibility and reliability of this method for gas sensing application. Furthermore, we measured the scatters around the straight line fits in Figure 9b,c,d,e. The slopes of the linear fit curves are 1.35 × 10^{-8}, 1.77 × 10^{-8}, 1.45 × 10^{-8}, and 1.55 × 10^{-8} cm^{-1}/ppmv, respectively. The standard deviations of the residual spectra are 4.02 × 10^{-7}, 3.29 × 10^{-7}, 3.41 × 10^{-7}, and 3.91 × 10^{-7} cm^{-1}, respectively. Therefore, the precisions are determined to be 29.7, 18.5, 23.5, and 25.2 ppmv, respectively. In this manner, the averaged precision is 24.2 ppmv, which is a little better than ~28.4 ppmv.

The sensitivity (α_{min}) of a sensor system is principally determined by the effective absorption path length (L_{eff}) of the cavity, which is mainly related to the mirror reflectivity and cavity length. Though there are differences in sensitivity and effective absorption path length, the noise level of a sensor system can be characterized by a proper indicator, i.e., the minimum detectable absorption (MDA, α_{min} × L_{eff}). The reported sensor by Denzer et al.[15] achieved an α_{min} of 6.1 × 10^{-8} cm^{-1} and an L_{eff} of 1250 m using the dispersive spectrometer with the absorption of 1,3-butadiene (C_4H_6, with an average cross section of ~1 × 10^{-21} cm^2/molecules), corresponding to an MDA of 7.625 × 10^{-3}. In this work, an MDA of 2.275 × 10^{-3} was obtained with an α_{min} of 1.85 × 10^{-6} cm^{-1} and an L_{eff} of 12.3 m on the absorption of CH_4 (with an average cross section of ~1.3 × 10^{-21} cm^2/molecules) using a scanning spectrometer. Therefore, the proposed sensor has a similar noise level with the sensor reported by Denzer et al.

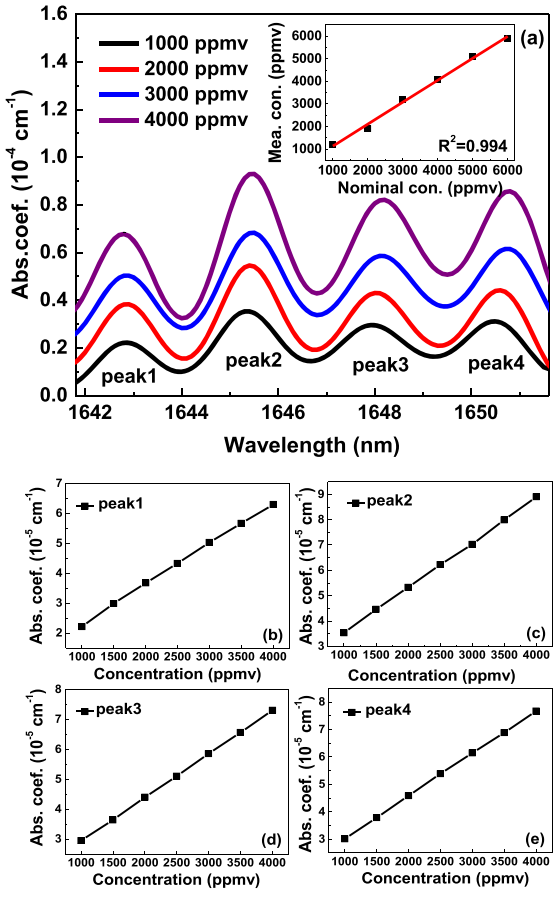

Figure 9. (a) Measured CH_4 absorption coefficient with different concentration levels and the inset shows the correlation plot of the measured concentration versus nominal value. Relationships between the maximum absorption coefficient (α_{max}) of (b) peak1, (c) peak2, (d) peak3, and (e) peak4 and the CH_4 concentration level, respectively.

COMPARISON AND DISCUSSION

Two detection schemes, i.e., NIRQuest spectrometry and scanning spectrometry, are demonstrated in NIR-IBBCEAS measurements, and a performance comparison between these two experimental methods is demonstrated in Table 1. Using the NIRQuest spectrometer, a SNR of 40 and a LoD (1σ) of 120 ppmv were obtained for a 1 s averaging time, and the LoD can be further improved to 19.4 ppmv for an averaging time of 45 s. Using the scanning spectrometer, a SNR of 162 and a

Table 1. Performance Comparison of the NIR-IBBCEAS Sensor System Using NIRQuest Spectrometer and Scanning Spectrometer, Respectively

Detection method	Spectral resolution (nm)	SNR	1σ LoD (ppmv)	Averaging time
NIRQuest	7.6	40	120	1 s
			19.4	45 s
Scanning + Lock-in	0.4	162	28.4	8 min

DOI: 10.1021/acssensors.9b00788
ACS Sens. 2019, 4, 1899−1908

Table 2. Performance Comparison among This Sensor and Previously Reported NIR-IBBCEAS Setups

ref	Source (Power)/ Method[a]	L (cm)	R	L_{eff} (m)	Sensitivity (cm^{-1})	Spectral range (nm) /resolution	Acquisition time	MDA(Target gas)
15	SLED (10 mW)/a	25	99.98%	1250	6.1×10^{-8}	1610−1700/15 cm^{-1}	6 min	7.625×10^{-3} (C_4H_6)
	SLED (10 mW)/b				1.5×10^{-8}	1610−1700/16 cm^{-1}	4 min	1.875×10^{-3} (C_4H_6)
16	SC (4W)/b	25	99.98%	1250	4×10^{-9}	1610−1700/4 cm^{-1}	4 min	5×10^{-4} (CH_4)
	SLED(10 mW) /b				2×10^{-8}			2.5×10^{-3} (C_3H_6O)
17	SC (2W)/b	644	99.9%	6440	8×10^{-8}	1215−1695/0.08 cm^{-1}	120 min	5.15×10^{-2} ($C_4H_8O_2$)
20	SC (800 mW)/c	117	99.997%	40 000	7.3×10^{-10}	1595−1620/0.1 nm	2.5 min	2.92×10^{-3} (CO_2)
	SLED (17 mW)/c				2.1×10^{-9}			8.4×10^{-3} (CO_2)
This paper	LED (16 mW)/d	8	99.35%	12.3	1.25×10^{-6}	1610−1690/7.6 nm	45 s	1.53×10^{-3} (CH_4)
	LED (16 mW)/a				1.85×10^{-6}	1630−1680/0.4 nm	8 min	2.27×10^{-3} (CH_4)

[a]Method a, using scanning spectrometer in combination with lock-in detection; Method b, using Fourier-transform spectrometer (FTS); Method c, using optical spectrum analyzer; Method d, using NIRQuest InGaAs spectrometer.

Table 3. Comparison among the Performances of This Sensor for CH_4 Detection and Those of Other Reported Techniques

ref	Technique	Light source	L_{eff} (m)	Sensitivity (cm^{-1})	Acquisition time	MDA
28	CRDS	Laser	2600	1.5×10^{-8}	15 min	3.9×10^{-3}
29	HC-PBF	Laser	5.1	1.57×10^{-6}	9.5 min	8×10^{-4}
30	TDLAS	Laser	30	6.17×10^{-7}	5 s	1.85×10^{-3}
31	QEPAS	Laser	/	1.6×10^{-7}	1 s	/
18	NIR-IBBCEAS	Halogen lamp	667	4.6×10^{-7}	20 min	3.07×10^{-2}
19	NIR-IBBCEAS	Halogen lamp	590	9.7×10^{-7}	30 s	5.75×10^{-2}
This paper	NIR-IBBCEAS	LED	12.3	1.25×10^{-6}	45 s[a]	1.53×10^{-3}
				1.85×10^{-6}	8 min[b]	2.27×10^{-3}

[a]Using NIRQuest InGaAs spectrometer. [b]Using scanning spectrometer in combination with lock-in detection.

LoD (1σ) of 28.4 ppmv were achieved for a 8 min averaging time. With respect to the SNR level, the scanning spectrometer is enhanced by a factor of ∼4 compared with that of the NIRQuest spectrometer, which is due to the use of lock-in detection. This improves the measurement accuracy of the sensor even under a low SNR condition. Additionally, by optimizing the time constant, the spectrometer output can be much smoother, stronger, and more stable, and thus a higher sensitivity is obtained.

The NIRQuest spectrometer has the advantages of fiber-input, portability, short acquisition time, and easy averaging with a detector array, but at the expense of low measurement resolution. The detection precision can be improved by increasing the integration time and optimizing the averaging number. The scanning spectrometer possesses a higher optical resolution and sensitivity combining with the lock-in detection, but requires a longer acquisition time. Due to the monochromator scanning and long integration time needed for improving the SNR, the measurement time is limited to 6 nm/min. Further improvement in sensitivity and detection speed can be made by using a high-power LED, increasing the effective mirror diameter, and using a detector array in the inside of the monochromator.

As shown in Table 2, the performances of the LED-based NIR-IBBCEAS sensor are compared with previously reported NIR-IBBCEAS setups. Compared with other IBBCEAS sensors, although the effective optical path length of this sensor system is short (∼12.3 m), the MDA of the reported sensor (∼10^{-3}) is at the same level as that of the SC (∼10^{-4}−10^{-3}) and Halogen lamp (∼10^{-3}−10^{-2}) based sensors.

Table 3 demonstrates the comparison among the performances of this IBBCEAS sensor for CH_4 detection and other reported sensors using cavity ring-down spectroscopy (CRDS),[28] hollow-core photonic bandgap fiber (HC-PBF),[29] tunable diode laser absorption spectroscopy (TDLAS),[30] quartz-enhanced photoacoustic spectroscopy (QEPAS),[31] and NIR-IBBCEAS.[18,19] Compared with other techniques for CH_4 detection, the MDA of the reported NIR-IBBCEAS sensor is basically on the same order of magnitude as other sensors using CRDS, HC-PBF, TDLAS, and QEPAS. Furthermore, the LED source takes advantage of low cost, compact size, and long lifetime, and the fabricated portable cavity with a length of only 8 cm provides an absorption path length up to ∼12 m, which makes such sensors more suitable for field and portable deployment than the laser-based sensors. To achieve a 12 m path length in such a short cell, using a multipass configuration (e.g., Herriott) would require 150 passes, which is at the high end of what is possible using a multipass method, and almost certainly not achievable in such a low volume cell. In addition, by utilizing dielectric mirrors with higher reflectivity, a spectrometer with lower noise, and a light source with higher power, an increased sensitivity and improved detection limit could be further achieved.

MULTIGAS SENSING PERFORMANCE OF CH_4/C_2H_2

One major advantage of NIR-IBBCEAS compared to other spectroscopic techniques is the capability for multigas sensing over a wide bandwidth. We exploited this potential to carry out dual-gas detection of C_2H_2 and CH_4 over the highly reflective range of the cavity from 1510 to 1680 nm. In order to obtain a high measurement resolution and sensitivity, the lock-in detection assisted scanning spectrometer was adopted in this experiment. C_2H_2 and CH_4 samples with the concentration levels of 800 and 1000 ppmv passed through the cell simultaneously. The measured high-resolution C_2H_2 spectrum was fitted in the spectral range of 1510−1545 nm and CH_4 was modeled from 1630 to 1680 nm. Good agreement between the measured and the modeled absorption spectra of the two gas

DOI: 10.1021/acssensors.9b00788
ACS Sens. 2019, 4, 1899−1908

species is achieved, as depicted in Figure 10. Detailed fitting results are shown in the inset of Figure 10. The retrieved

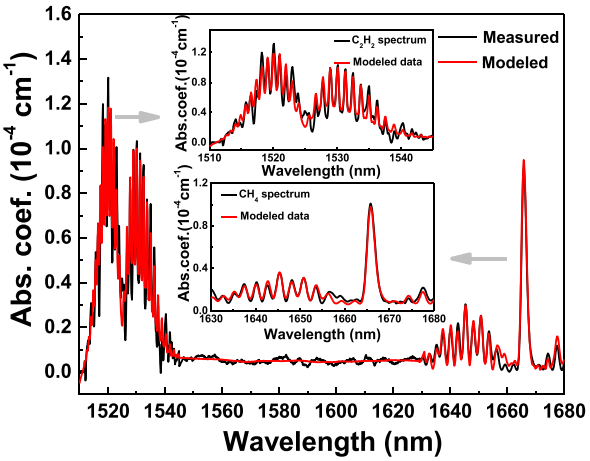

Figure 10. Simultaneous multigas sensing of 800 ppmv C_2H_2 (from 1510 to 1545 nm) and 1000 ppmv CH_4 (from 1630 to 1680 nm). The inset figure highlights the agreement between the measured (black line) and modeled (red line) spectra.

concentration levels were 832 and 1025 ppmv for C_2H_2 and CH_4 with an uncertainty of ~3.8% and ~2.5%, respectively.

FIELD EXPERIMENT OF MONITORING CH_4 GAS LEAKAGE

For field measurements, the NIR-IBBCEAS sensor was mounted on a cart and the power was supplied by a battery (CN5D0, Sail) connected to an AC inverter (7823N, NFA). The photograph shown in Figure 11a of the CH_4 sensor was taken when it was placed outside the State Key Laboratory of Integrated Optoelectronics on the Jilin University campus to monitor the variation of CH_4 concentration levels during CH_4 leakage. The CH_4 concentration level of the cylinder was 1%, and the distance between the leakage point and the CH_4 sensor was ~1 m. Gas leakage monitoring were conducted at an ambient temperature of 22 °C and a wind speed of 0.5 m/s. The integration time of the NIRQuest spectrometer was 100 ms and the data processing time of the LabVIEW platform was 0.2 s. Therefore, one concentration point was obtained per 0.3 s. As shown in Figure 11b, the sensor was turned on ahead of time, and the cylinder valve was opened at 49 s to simulate a CH_4 leakage. After 3 s of gas diffusion, the CH_4 concentration level monitored began to rise. Due to the influence of wind and the uncertainty of diffusion, the gas concentration still fluctuated in the process of approaching the maximum value after 62 s. This experiment proves the sensor's ability to detect CH_4 leakage in the field, which will be helpful for household natural gas leakage alarms and pipeline leakage monitoring of natural gas.

CONCLUSION

A broadband cavity-enhanced sensor system using an NIR LED as the light source was experimentally demonstrated. This is the first use of an energy-efficient InGaAs-LED in NIR-IBBCEAS. An ultraportable absorption gas cell with a volume of 42 mL was fabricated and an optical cavity with a physical length of 8 cm and a mirror reflectivity of 99.35% was developed. Dual-detection schemes using NIRQuest spectrometry and scanning spectrometry were adopted in the sensor system for performance evaluation. Sensitivities of 19.4 ppmv for a 45 s averaging time using the NIRQuest spectrometer and 28.4 ppmv for an 8 min averaging time using the scanning spectrometer in combination with lock-in detection were achieved. A field experiment of monitoring CH_4 leakage was performed using the fast-response NIRQuest spectrometer. Simultaneous detection of C_2H_2/CH_4:N_2 mixture was conducted using the high-resolution scanning spectrometer. Compared to the single-wavelength detection method, the demonstrated LED-based NIR-IBBCEAS sensor system provides better selectivity, flexibility, and potential for multicomponent analysis with a compact and cost-effective package. Further possibilities for ultrasensitive multicomponent measurements are to extend the technique to the mid-infrared spectral range, where strong absorption bands associated with fundamental vibrational transitions can be used.

ASSOCIATED CONTENT

Supporting Information

The Supporting Information is available free of charge on the ACS Publications website at DOI: 10.1021/acssensors.9b00788.

High-resolution spectrum of C_2H_2 and CH_4; the instrumental function for C_2H_2 and CH_4 convolution;

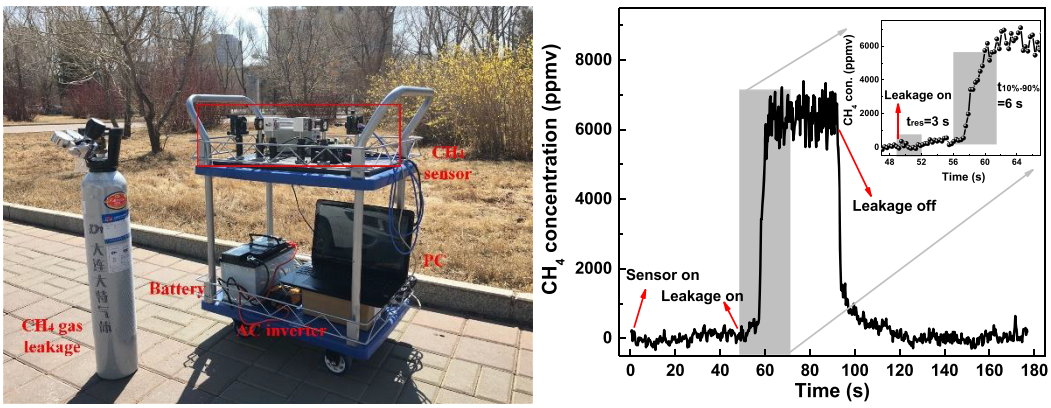

Figure 11. (a) NIR-IBBCEAS based CH_4 sensor installed on a laboratory cart on the campus of Jilin University. (b) Measured CH_4 concentration levels during a simulated CH_4 leakage.

DOI: 10.1021/acssensors.9b00788
ACS Sens. 2019, 4, 1899−1908

the convoluted cross section of C_2H_2 and CH_4; the calibrated highly reflective mirror's reflectivity (PDF)

AUTHOR INFORMATION

Corresponding Author

*E-mail: zhengchuantao@jlu.edu.cn.

ORCID

Kaiyuan Zheng: 0000-0002-5453-6770
Chuantao Zheng: 0000-0001-8008-466X
Yu Zhang: 0000-0003-2100-621X

Author Contributions

K.Z. performed the experiments and wrote the manuscript. C.Z. and Y.W supported the experiments. N.M, Z.L., and Y.Y. provided technical guidance. C.Z., Y.Z., and F.K.T. provided technical guidance and contributed to the manuscript. All authors discussed and commented on the manuscript.

Notes

The authors declare no competing financial interest.

ACKNOWLEDGMENTS

This work was supported in part by the National Key R&D Program of China (No. 2017YFB0405300), National Natural Science Foundation of China (Nos. 61775079, 61627823), Science and Technology Development Program of Jilin Province, China (Nos. 20180201046GX, 20190101016JH), Industrial Innovation Program of Jilin Province, China (No. 2017C027), and the National Science Foundation (NSF) ERC MIRTHE award and Robert Welch Foundation (No. C-0586).

REFERENCES

(1) Jin, W.; Cao, Y.; Yang, F.; Ho, H. L. Ultra-Sensitive All-Fibre Photothermal Spectroscopy with Large Dynamic Range. *Nat. Commun.* **2015**, *6*, 7767−7774.

(2) Zheng, C. T.; Ye, W. L.; Sanchez, N. P.; Li, C. G.; Dong, L.; Wang, Y. D.; Griffin, R. J.; Tittel, F. K. Development and Field Deployment of a Mid-Infrared Methane Sensor without Pressure Control Using Interband Cascade Laser Absorption Spectroscopy. *Sens. Actuators, B* **2017**, *244*, 365−372.

(3) Kiwanuka, S. S.; Laurila, T. K.; Frank, J. H.; Esposito, A.; Blomberg von der Geest, K.; Pancheri, L.; Stoppa, D.; Kaminski, C. F. Development of Broadband Cavity Ring-Down Spectroscopy for Biomedical Diagnostics of Liquid Analytes. *Anal. Chem.* **2012**, *84* (13), 5489−5493.

(4) Ren, W.; Luo, L.; Tittel, F. K. Sensitive Detection of Formaldehyde Using an Interband Cascade Laser near 3.6 μm. *Sens. Actuators, B* **2015**, *221*, 1062−1068.

(5) Wu, H. P.; Dong, L.; Zheng, H. D.; Yu, Y. J.; Ma, W. G.; Zhang, L.; Yin, W. B.; Xiao, L. T.; Jia, S. T.; Tittel, F. K. Beat Frequency Quartz-Enhanced Photoacoustic Spectroscopy for Fast and Calibration-Free Continuous Trace-Gas Monitoring. *Nat. Commun.* **2017**, *8*, 15331−15338.

(6) Zheng, C. T.; Ye, W. L.; Li, G. L.; Yu, X.; Zhao, C. X.; Song, Z. W.; Wang, Y. D. Performance Enhancement of a Mid-Infrared CH_4 Detection Sensor by Optimizing an Asymmetric Ellipsoid Gas-Cell and Reducing Voltage-Fluctuation: Theory Design and Experiment. *Sens. Actuators, B* **2011**, *160*, 389−398.

(7) Li, B.; Zheng, C. T.; Liu, H. F.; He, Q. X.; Ye, W. L.; Zhang, Y.; Pan, J. Q.; Wang, Y. D. Development and Measurement of a Near-Infrared CH_4 Detection System Using 1.654 μm Wavelength-Modulated Diode Laser and Open Reflective Gas Sensing Probe. *Sens. Actuators, B* **2016**, *225*, 188−198.

(8) Zheng, K. Y.; Zheng, C. T.; He, Q. X.; Yao, D.; Hu, L. E.; Zhang, Y.; Wang, Y. D.; Tittel, F. K. Near-Infrared Acetylene Sensor System Using Off-Axis Integrated-Cavity Output Spectroscopy and Two Measurement Schemes. *Opt. Express* **2018**, *26* (20), 26205−26216.

(9) Fiedler, S. E.; Hese, A.; Ruth, A. A. Incoherent Broad-Band Cavity-Enhanced Absorption Spectroscopy. *Chem. Phys. Lett.* **2003**, *371*, 284−294.

(10) Venables, D. S.; Gherman, T.; Orphal, J.; Wenger, J. C.; Ruth, A. A. High Sensitivity In−Situ Monitoring of NO_3 in an Atmospheric Simulation Chamber Using Incoherent Broadband Cavity−Enhanced Absorption Spectroscopy. *Environ. Sci. Technol.* **2006**, *40* (21), 6758−6763.

(11) Zheng, K. Y.; Zheng, C. T.; Zhang, Y.; Wang, Y. D.; Tittel, F. K. Review of Incoherent Broadband Cavity-Enhanced Absorption Spectroscopy (IBBCEAS) for Gas Sensing. *Sensors* **2018**, *18*, 3646−3670.

(12) Wu, T.; Zha, Q. Z.; Chen, W. D.; Zheng, X.; Wang, T.; He, X. D. Development and Deployment of a Cavity Enhanced UV-LED Spectrometer for Measurements of Atmospheric HONO and NO_2 in Hong Kong. *Atmos. Environ.* **2014**, *95*, 544−551.

(13) Fang, B.; Zhao, W. X.; Xu, X. Z.; Zhou, J. C.; Ma, X.; Wang, S.; Zhang, W. J.; Venables, D. S.; Chen, W. D. Portable Broadband Cavity-Enhanced Spectrometer Utilizing Kalman Filtering: Application to Real-Time, in Situ Monitoring of Glyoxal and Nitrogen Dioxide. *Opt. Express* **2017**, *25* (22), 26910−26922.

(14) Orphal, J.; Ruth, A. A. High-Resolution Fourier-Transform Cavity-Enhanced Absorption Spectroscopy in the Near-Infrared Using an Incoherent Broad-Band Light Source. *Opt. Express* **2008**, *16* (23), 19232−19243.

(15) Denzer, W.; Hamilton, M. L.; Hancock, G.; Islam, M.; Langley, C. E.; Peverall, R.; Ritchie, G. A. D. Near-infrared Broad-Band Cavity Enhanced Absorption Spectroscopy Using a Superluminescent Light Emitting Diode. *Analyst* **2009**, *134* (11), 2220−2223.

(16) Denzer, W.; Hancock, G.; Islam, M.; Langley, C. E.; Peverall, R.; Ritchie, G. A. D.; Taylor, D. Trace Species Detection in the Near Infrared Using Fourier Transform Broadband Cavity Enhanced Absorption Spectroscopy: Initial Studies on Potential Breath Analytes. *Analyst* **2011**, *136* (4), 801−806.

(17) Chandran, S.; Varma, R. Near Infrared Cavity Enhanced Absorption Spectra of Atmospherically Relevant Ether-1, 4-Dioxane. *Spectrochim. Acta, Part A* **2016**, *153*, 704−708.

(18) Prakash, N.; Ramachandran, A.; Varma, R.; Chen, J.; Mazzoleni, C.; Du, K. Near-Infrared Incoherent Broadband Cavity Enhanced Absorption Spectroscopy (NIR-IBBCEAS) for Detection and Quantification of Natural Gas Components. *Analyst* **2018**, *143*, 3284−3291.

(19) Zheng, K. Y.; Zheng, C. T.; Liu, Z. D.; He, Q. X.; Du, Q. L.; Zhang, Y.; Wang, Y. D.; Tittel, F. K. Near-Infrared Broadband Cavity-Enhanced Sensor System for Methane Detection Using a Wavelet-Denoising Assisted Fourier-Transform Spectrometer. *Analyst* **2018**, *143*, 4699−4706.

(20) Aalto, A.; Genty, G.; Laurila, T.; Toivonen, J. Incoherent Broadband Cavity Enhanced Absorption Spectroscopy Using Supercontinuum and Superluminescent Diode Sources. *Opt. Express* **2015**, *23* (19), 25225−25234.

(21) Langridge, J. M.; Laurila, T.; Watt, R. S.; Jones, R. L.; Kaminski, C. F.; Hult, J. Cavity Enhanced Absorption Spectroscopy of Multiple Trace Gas Species Using a Supercontinuum Radiation Source. *Opt. Express* **2008**, *16* (14), 10178−10188.

(22) Yu, S. Y.; Yan, L.; Zhang, T. Q.; Zhang, Y.; Zhang, X. Y.; Sun, G.; Yu, W. W. Gas Detection Based on Quantum Dot Leds utilizing Differential Optical Absorption Spectroscopy. *RSC Adv.* **2017**, *7* (48), 30096−30100.

(23) Wang, Y.; Bai, X.; Wang, T. Y.; Yan, L.; Zhang, T. Q.; Zhang, Y.; Yu, W. W. Efficient Near-Infrared Light-Emitting Diodes Based on Liquid Pbse Quantum Dots. *Nanotechnology* **2017**, *28* (21), 215703−215710.

(24) Zhang, Y.; Yang, J.; Hou, Q.; Mo, Y. Q.; Peng, J. B.; Cao, Y. Near Infrared Polymer Light-Emitting Diodes. *Chin. Sci. Bull.* **2005**, *50* (10), 957−960.

DOI: 10.1021/acssensors.9b00788
ACS Sens. 2019, 4, 1899−1908

(25) Kohring, M.; Bottger, S.; Willer, U.; Schade, W. LED-Absorption-QEPAS Sensor for Biogas Plants. *Sensors* **2015**, *15* (5), 12092−12102.
(26) Bogomolov, A.; et al. Development and Testing of an LED-Based Near-infrared Sensor for Human Kidney Tumor Diagnostics. *Sensors* **2017**, *17* (8), 1914−1930.
(27) Varma, R. M.; Venables, D. S.; Ruth, A. A.; Heitmann, U.; Schlosser, E.; Dixneuf, S. Long Optical Cavities for Open-Path Monitoring of Atmospheric Trace Gases and Aerosol Extinction. *Appl. Opt.* **2009**, *48* (4), 159−171.
(28) Fawcett, B. L.; Parkes, A. M.; Shallcross, D. E.; Orrewing, A. J. Trace Detection of Methane Using Continuous Wave Cavity Ring-Down Spectroscopy at 1.65 μm. *Phys. Chem. Chem. Phys.* **2002**, *4*, 5960−5965.
(29) Cubillas, A. M.; Lazaro, J. M.; Conde, O. M.; Petrovich, M. N.; Lopez-Higuera, J. M. Gas Sensor Based on Photonic Crystal Fibres in the $2\nu_3$ and $\nu_2 + 2\nu_3$ Vibrational Bands of Methane. *Sensors* **2009**, *9*, 6261−6272.
(30) Stachowiak, D.; Jaworski, P.; Krzaczek, P.; Maj, G.; Nikodem, M. Laser-based Monitoring of CH_4, CO_2, NH_3 and H_2S in Animal Farming-system Characterization and Initial Demonstration. *Sensors* **2018**, *18*, 529−540.
(31) Dong, L.; Wright, J.; Peters, B.; Ferguson, B. A.; Tittel, F. K.; McWhorter, S. Compact QEPAS Sensor for Trace Methane and Ammonia Detection in Impure Hydrogen. *Appl. Phys. B: Lasers Opt.* **2012**, *107* (2), 459−467.

DOI: 10.1021/acssensors.9b00788
ACS Sens. 2019, 4, 1899−1908